Supplement: Determining the Optimal Grid Resolution for Topographic Analysis on an Airborne Lidar Dataset

Taylor Smith[1], Aljoscha Rheinwalt[1], and Bodo Bookhagen[1]

[1]Institute of Earth and Environmental Sciences, Universität Potsdam, Germany

Correspondence: Taylor Smith (tasmith@uni-potsdam.de)

1 Data and Methods

As a second synthetic figure, we generate a sphere with a radius of one, with elevations defined as $z = \sin(\arccos(\sqrt{x^2 + y^2}))$. The following figures contain both the Gaussian hill data and the sphere data.

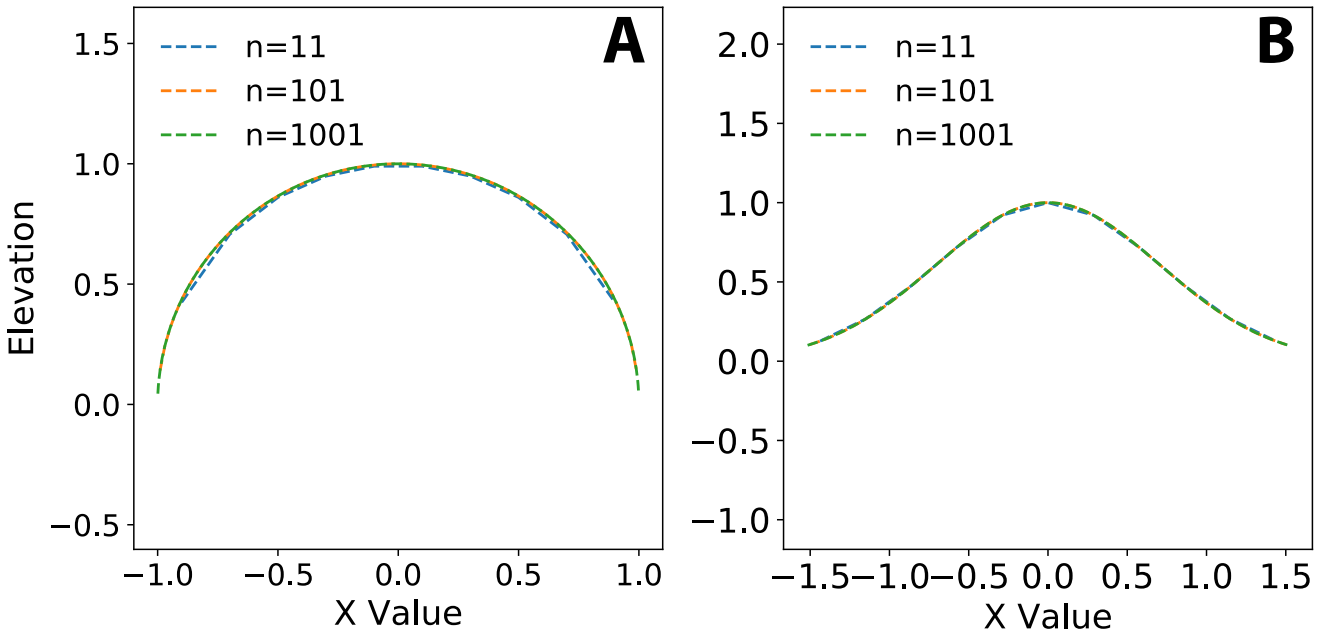

Figure S1. Sphere (left) and Gaussian Hill (right) elevations at n=11, 101, and 1001 in profile.

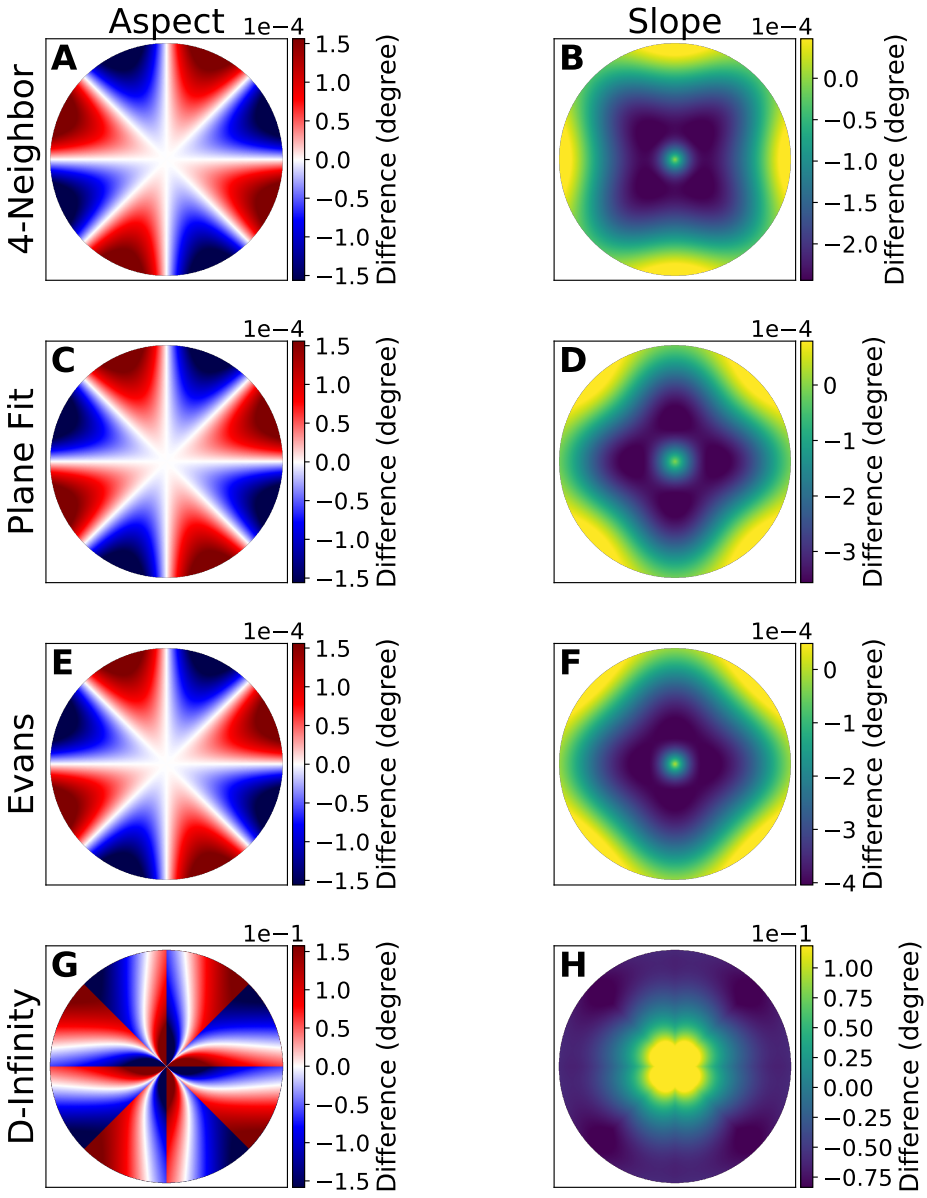

Figure S2. Absolute offset from the analytical solution for slopes and aspects on a Gaussian Hill (n=1001) for (1) 4-neighbor method, (2) plane fits, (3) Evans (*Evans, 1980*) method, and (4) D-Infinity (*Tarboton, 1997*). Colors scaled from 5th to 95th percentiles.

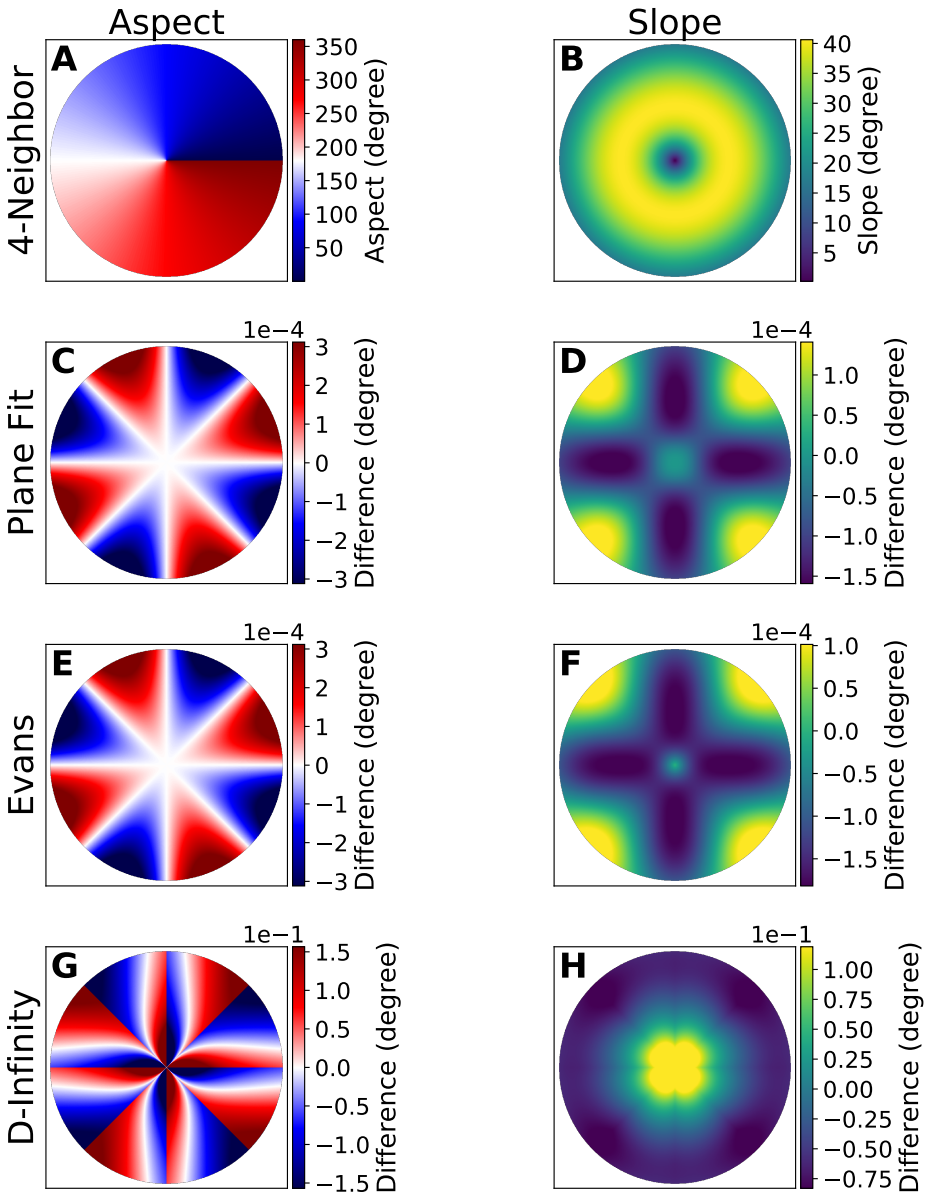

Figure S3. Slope and Aspect for a Gaussian Hill (n=1001) using four different methods. (1) 4-neighbor method, (2) difference between plane fits and 4-neighbor method, (3) difference between Evans (*Evans, 1980*) method and 4-neighbor method, and (4) difference between D-Infinity (*Tarboton, 1997*) and 4-neighbor method. Colors scaled from 5th to 95th percentiles.

2 Sources of Error in Topographic Metrics

2.1 Truncation Error

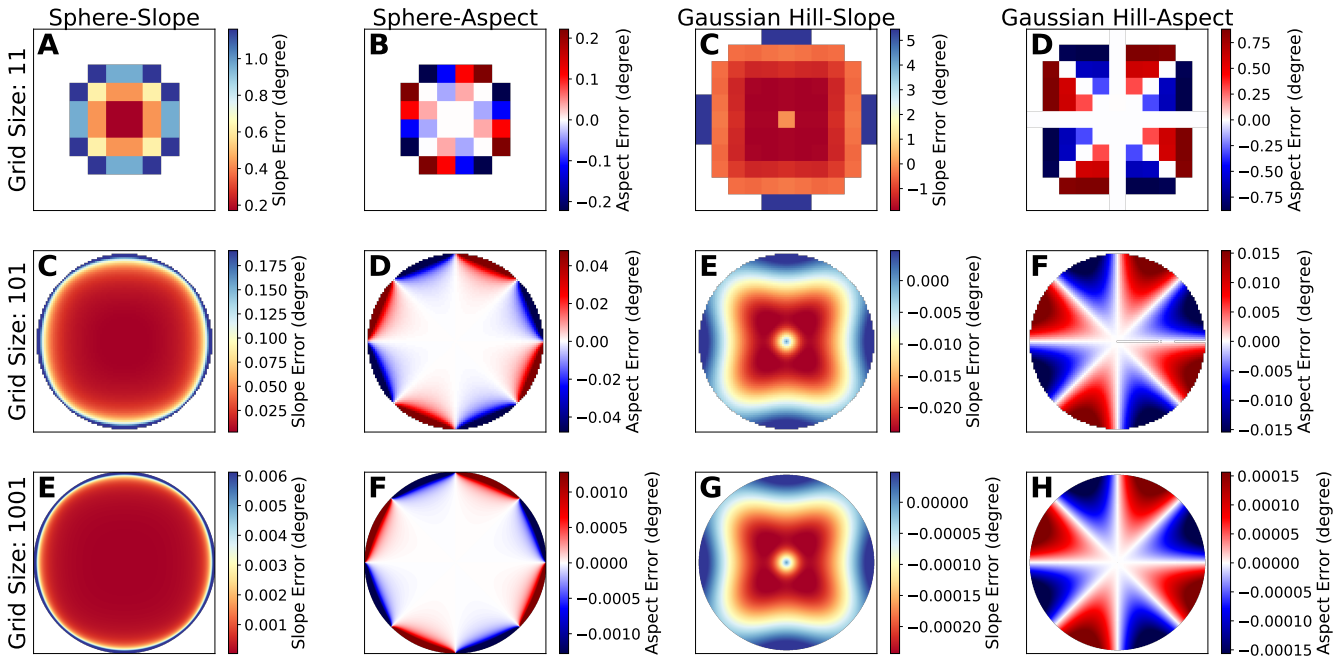

Figure S4. Sphere (left) and Gaussian Hill (right) aspect and slope differences from experimental comparison between calculated and perfect terrain derivatives. Both shapes show clear spatial patterns in slope and aspect biases. While the aspect bias patterns are similar for both shapes, slope differences show distinctly different spatial patterns. Offset magnitudes are generally similar between both shapes, and scale with grid resolution. Colors scaled from 5th to 95th percentiles.

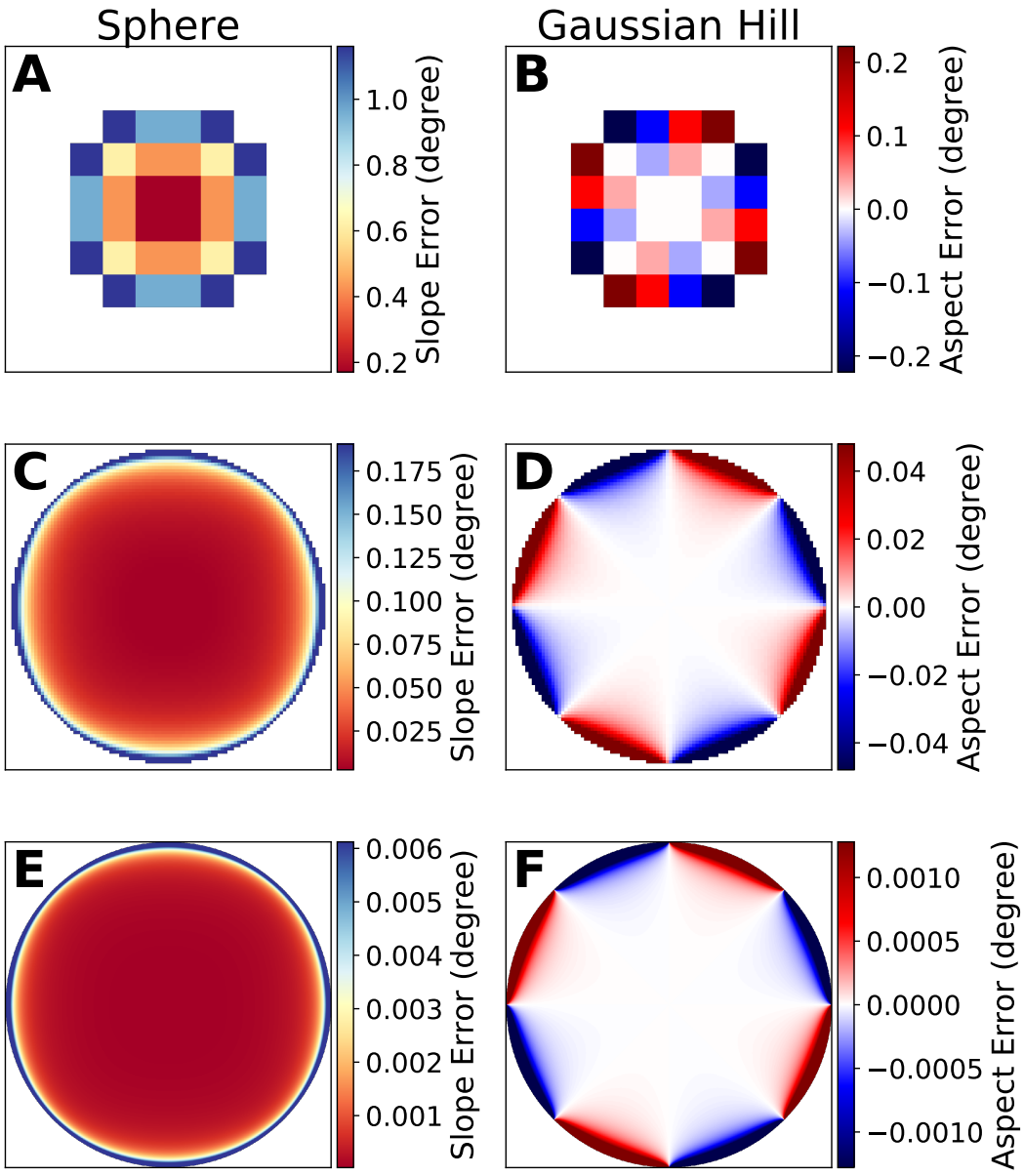

Figure S5. Sphere aspect and slope differences from a mathematically perfect surface, where sphere radius increases with grid size. Spatial and magnitude patterns of offsets are similar between a sphere of fixed radius and one with an increasing radius (cf. Supplemental Figure S4).

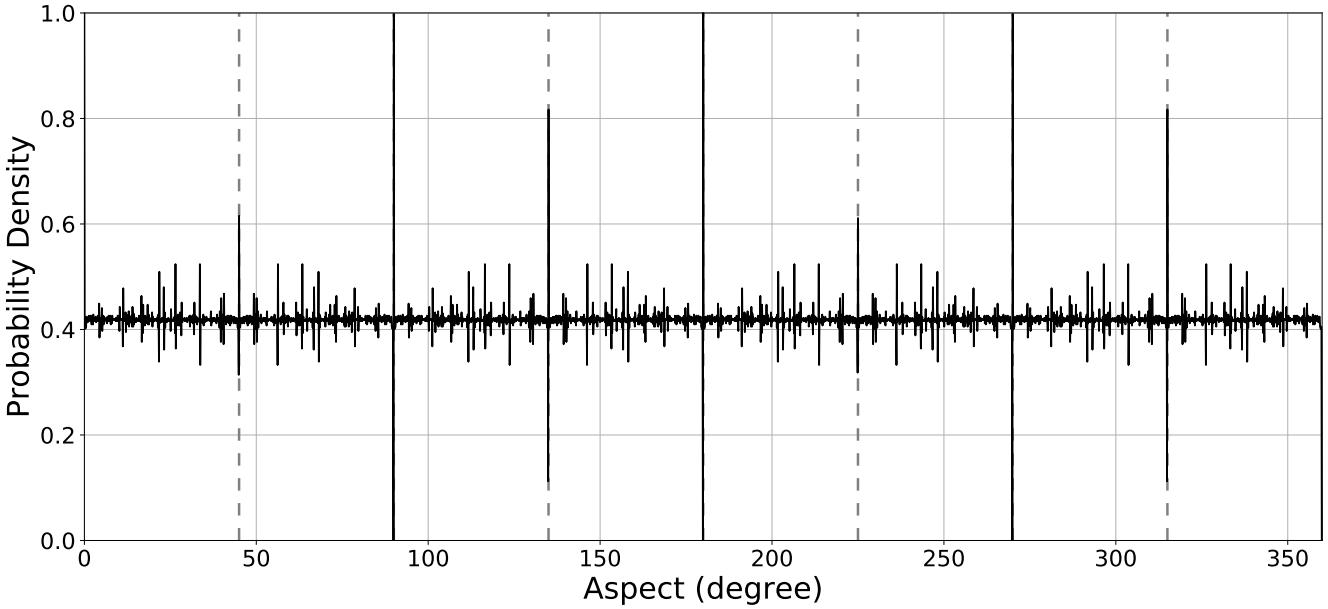

Figure S6. Aspect histogram for a Gaussian hill (n=1001), with fine (0.1 degree) aspect bins. Clear positive and negative harmonics throughout the distribution, with the largest 'spikes' around the cardinal directions.

2.2 DEM Uncertainty

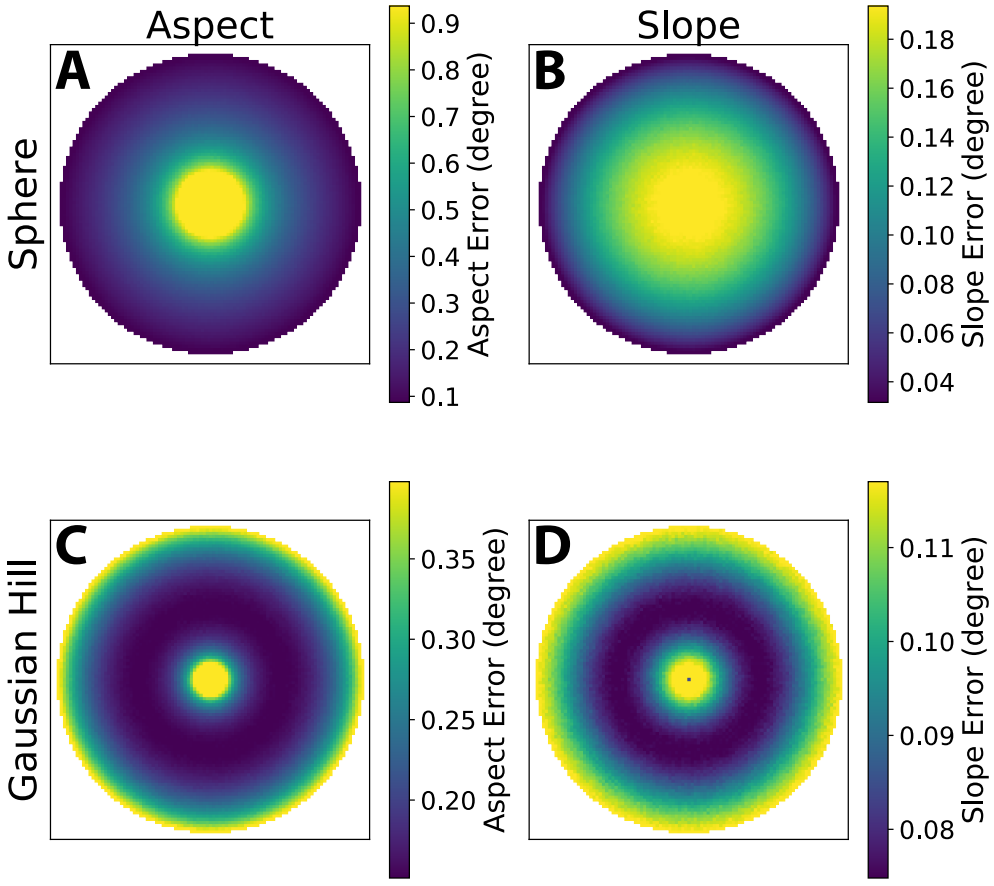

Figure S7. Sphere (left) and Gaussian hill (right) aspect and slope standard deviations for a given noise level, derived from an ensemble of generated DEMs with normally distributed noise (ensemble size, n=10,000). Noise STD = $1e^{-4}$.

3 Optimal Grid Spacing

3.1 Metric Quality Ratios

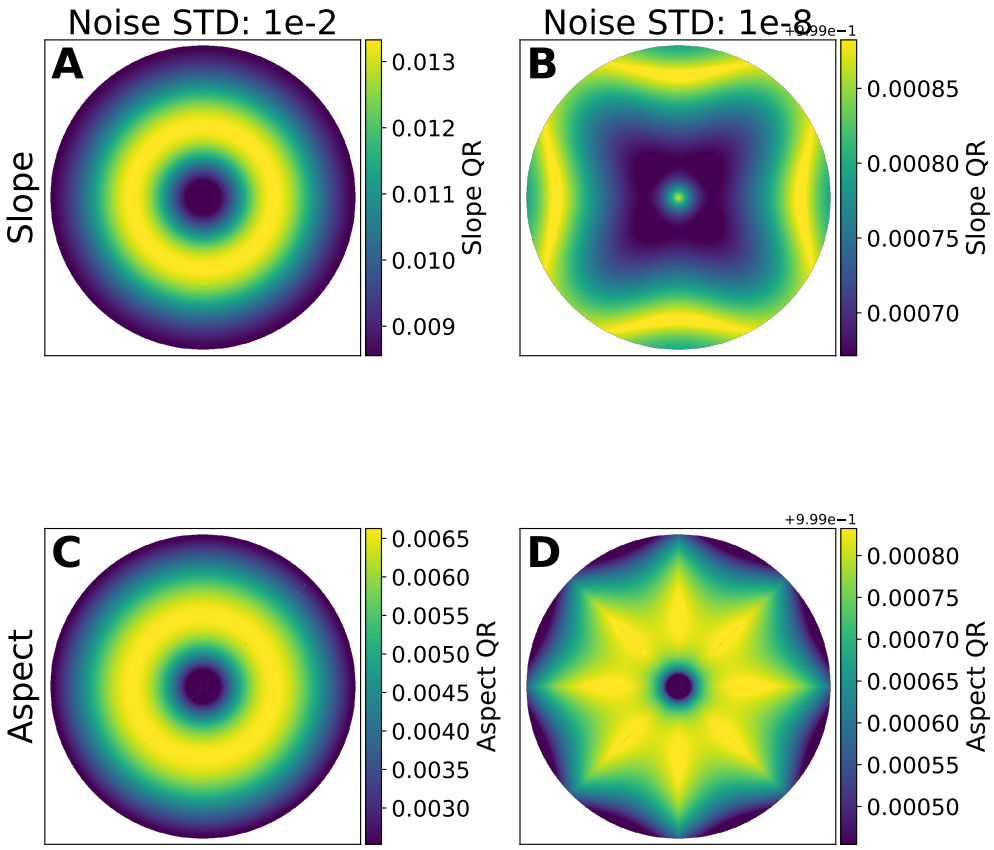

Figure S8. Slope (top) and aspect (bottom) quality ratios for noise standard deviations $1e^{-2}$ (left) and $1e^{-8}$ (right). High noise levels lead to error patterns dominated by PEU. Low noise shows the influence of truncation error on the spatial error pattern.

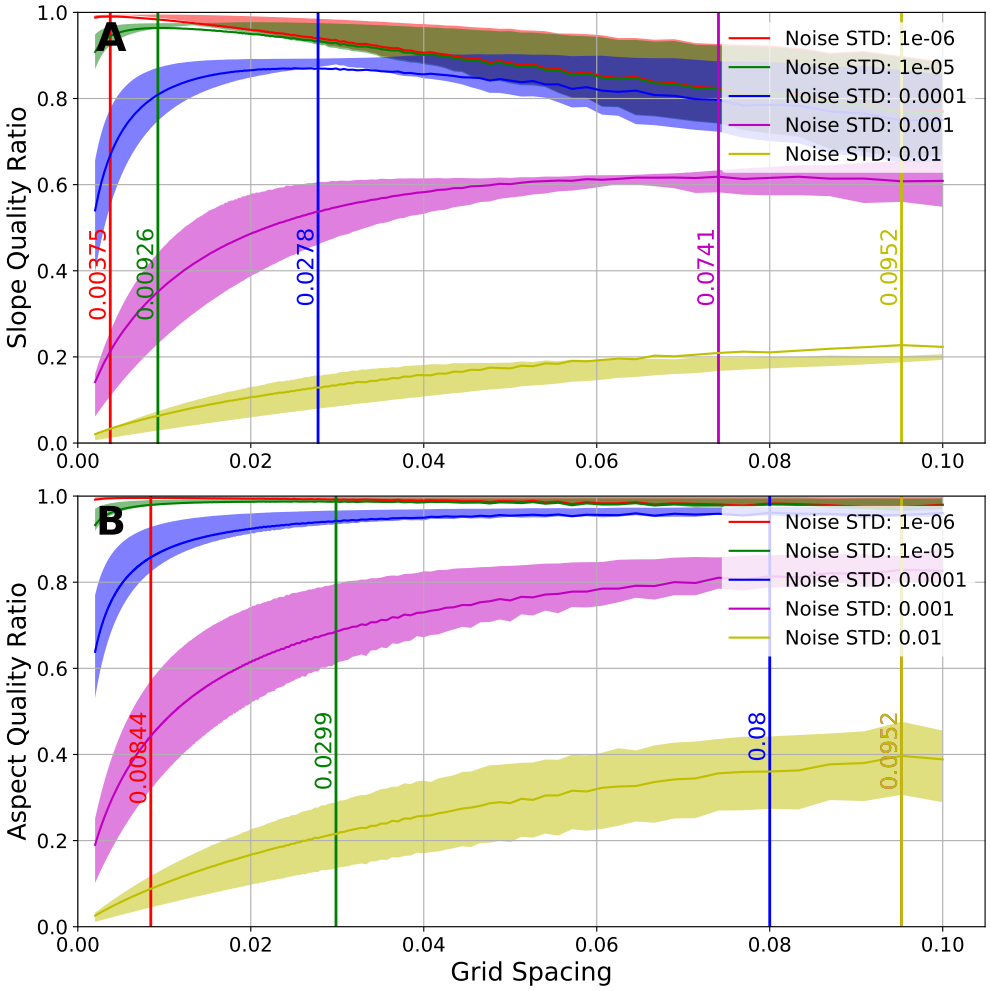

Figure S9. Sphere aspect (top) and slope (bottom) QRs vs grid spacings, for a range of noise levels ($1e^{-2}$ to $1e^{-6}$). 25th-75th percentile QRs shaded for each noise level. Optimal grid resolutions (maximum QR) for each noise level are marked with vertical lines. Slope calculations result in lower optimal grid spacings compared to aspect, because of higher QRs for slope. Higher noise levels lead to higher optimal grid spacings for both slope and aspect calculations. Note that the purple and yellow lines in panel B have the same ideal grid spacing, and thus only the yellow line is visible.

3.2 Heterogeneous Noise

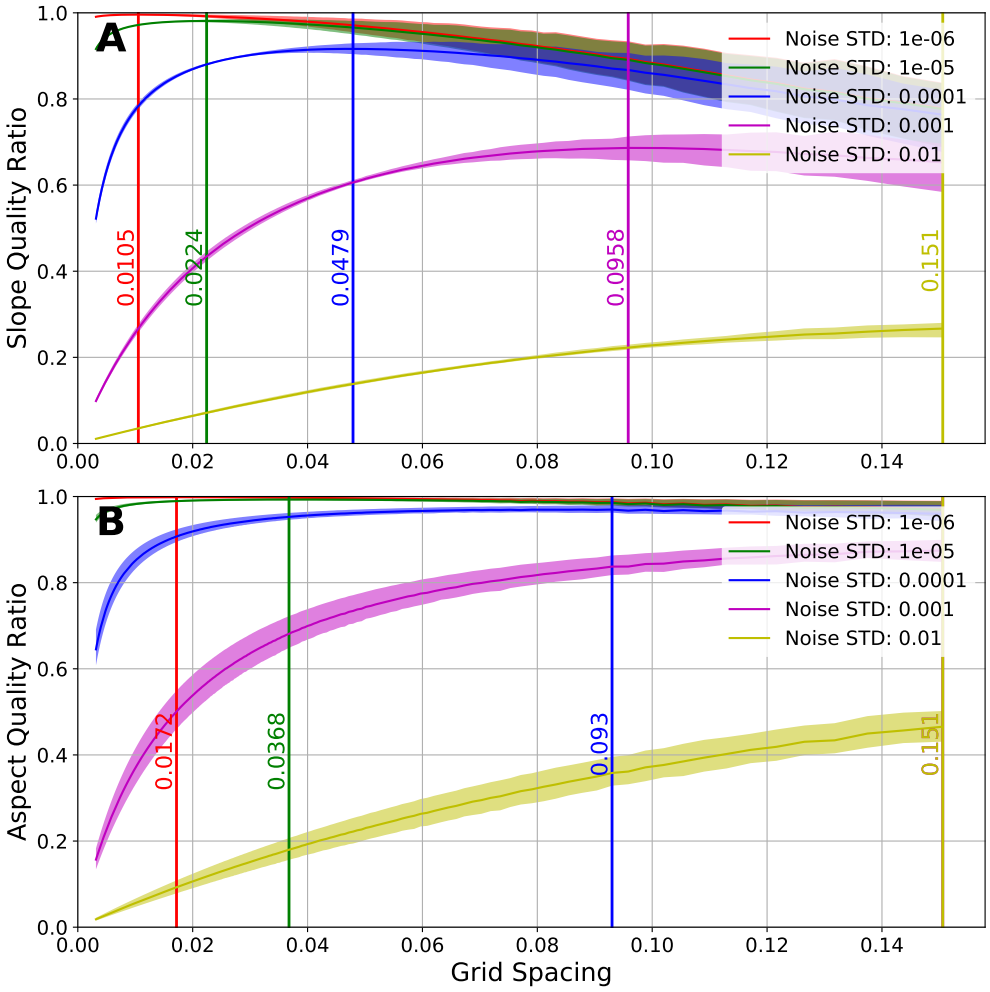

Figure S10. Gaussian hill grid spacing vs QR for varying noise levels biased by slope. 25th-75th percentile QRs shaded. Optimal grid resolution (max QR) marked with vertical lines. Note that the purple and yellow lines in panel B have the same ideal grid spacing, and thus only the yellow line is visible.

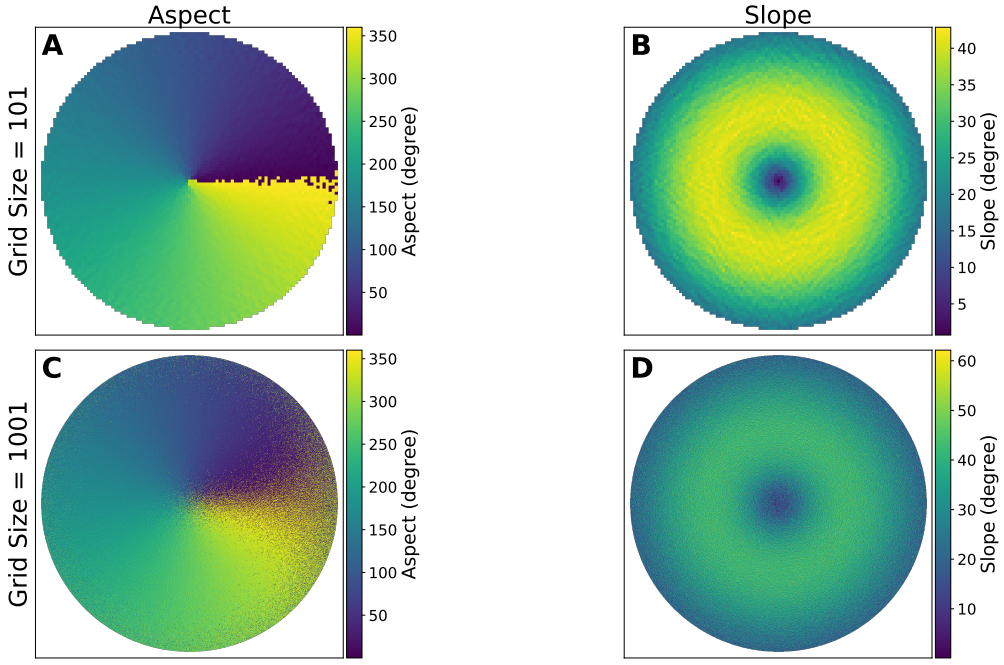

Figure S11. Images showing the Gaussian hill slope and aspect grids with added noise (mean=0, std=$1e^{-3}$) for n=101 (top) and n=1001 (bottom).

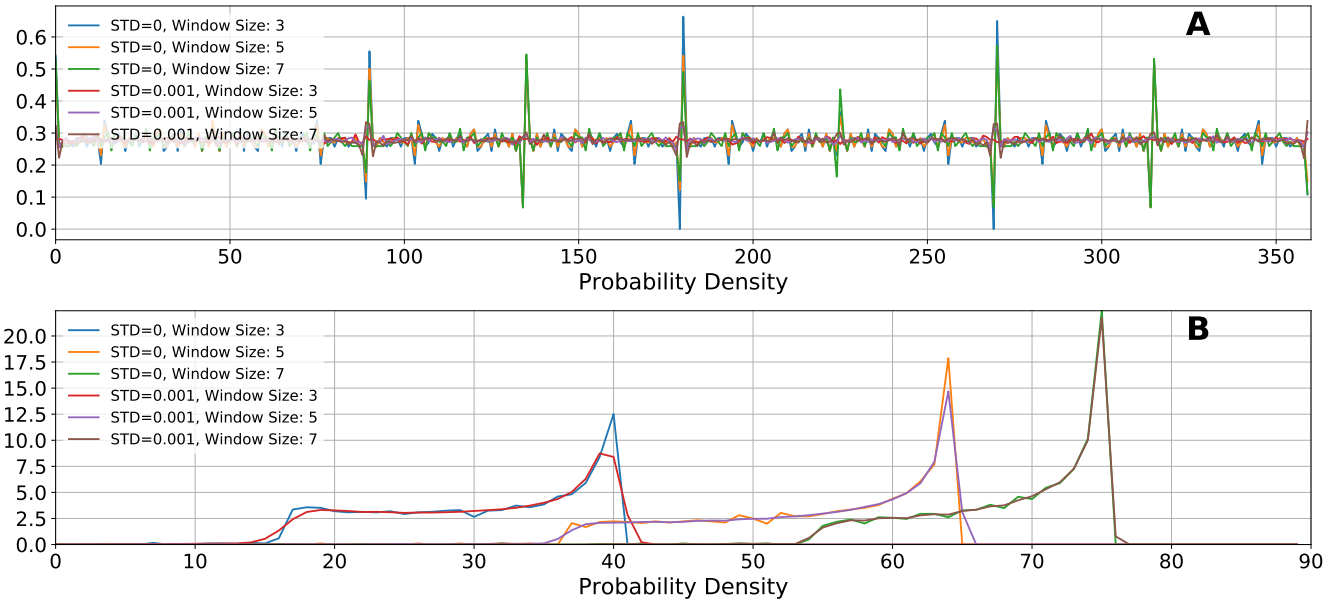

Figure S12. Slope and aspect distributions for a Gaussian hill with variable noise levels and window sizes.

5 Case Study: Multi-Resolution Lidar on Santa Cruz Island

5.1 Dataset Description

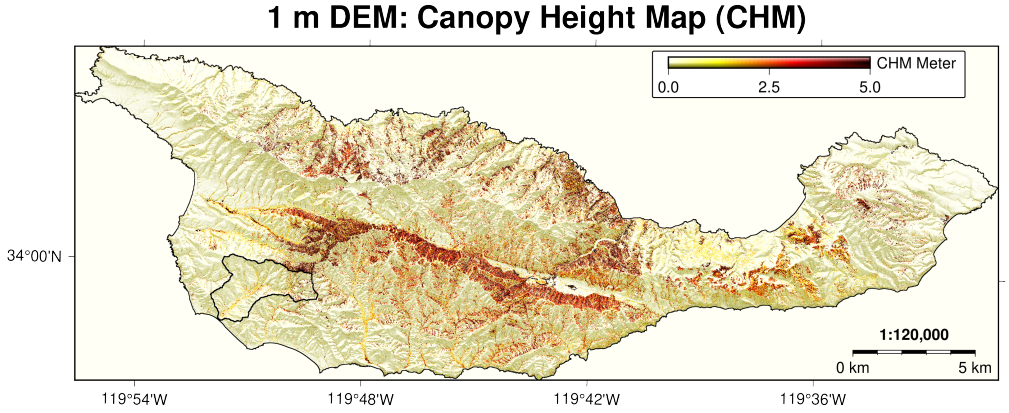

Figure S13. Island-wide canopy-height model, derived from a one meter DEM (cf. Figure 10). Vegetation heights are generally low, excepting some central regions of SCI.

5.2 Deriving Elevations and Elevation Uncertainties

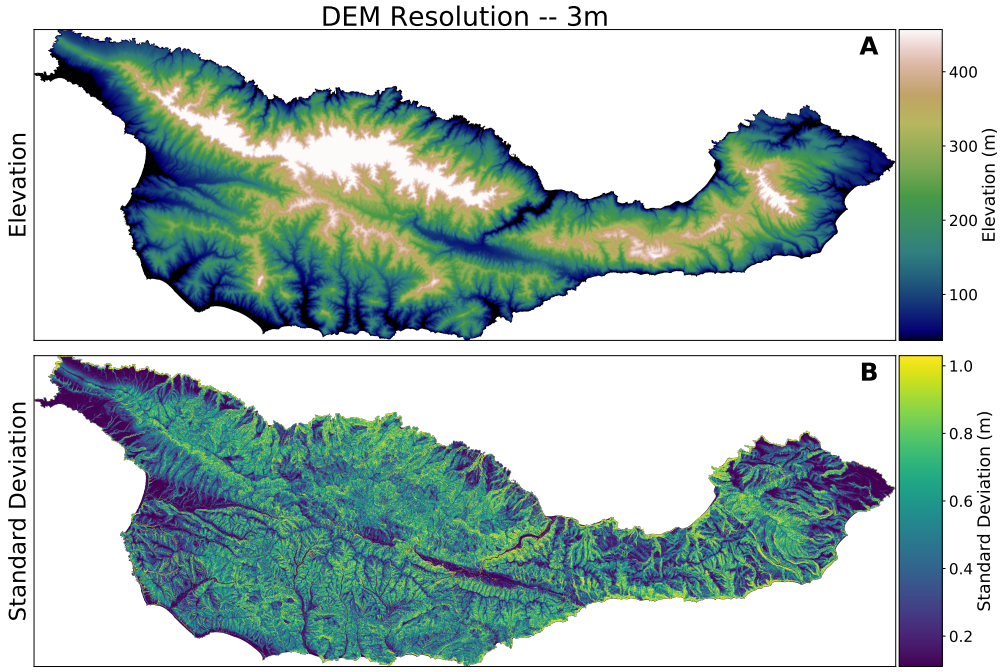

Figure S14. SCI elevation and standard deviation – 3m spatial resolution.

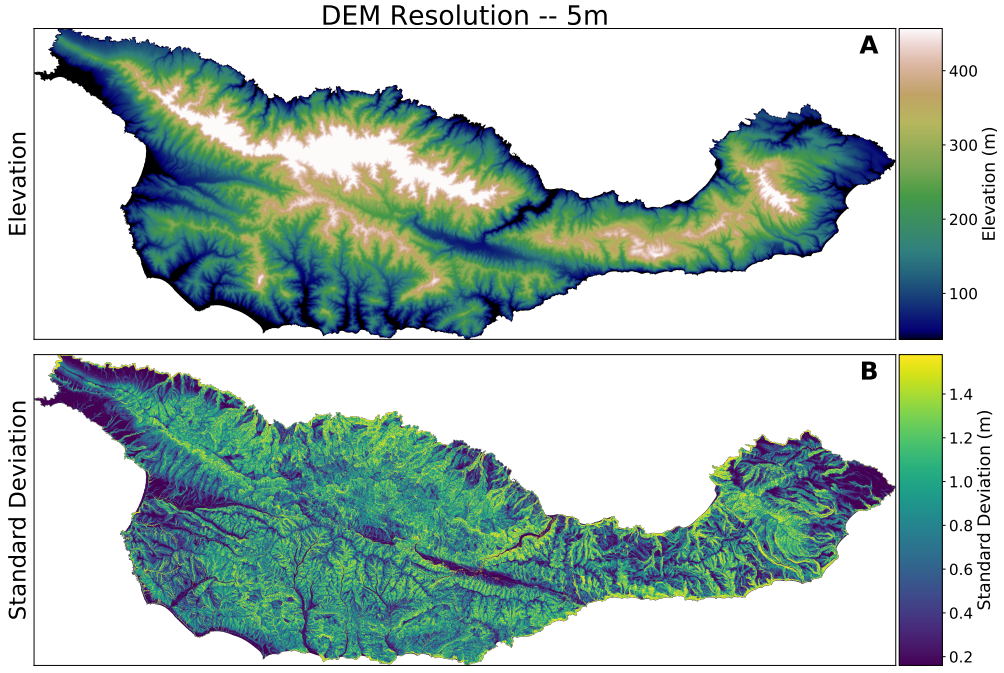

Figure S15. SCI elevation and standard deviation – 5m spatial resolution.

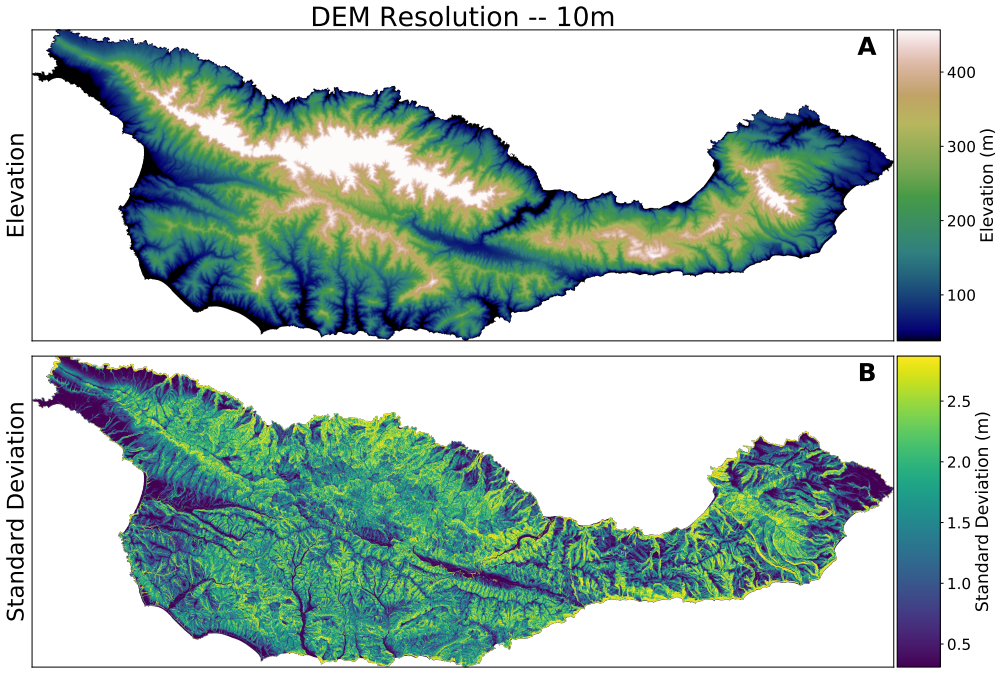

Figure S16. SCI elevation and standard deviation – 10m spatial resolution.

5.3 Mapping Uncertainty on SCI

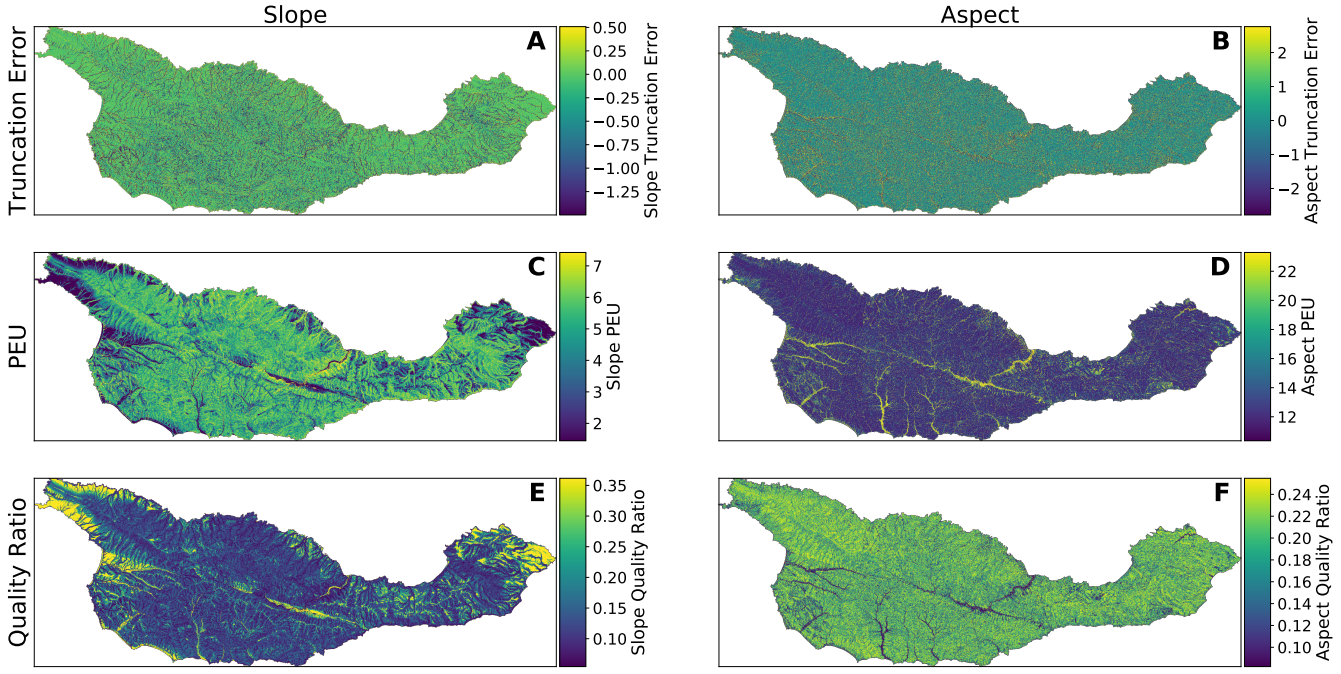

Figure S17. Truncation error (top), PEU (middle), and QR (bottom) for slope (left) and aspect (right) across the entire SCI, calculated from 5m data. Both truncation and PEU are higher for aspect, leading to much lower QRs.

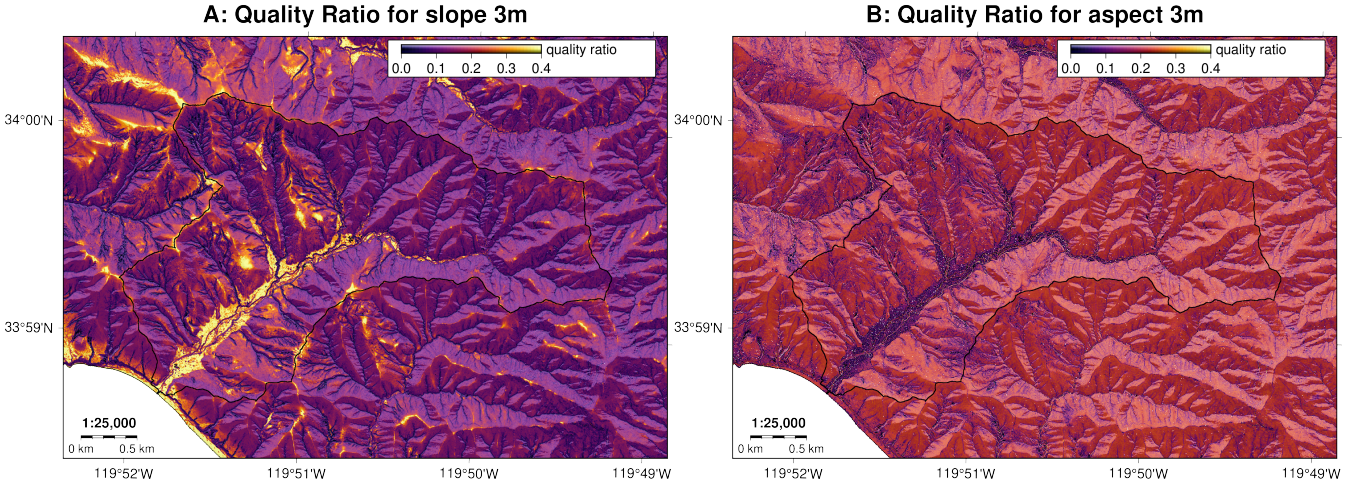

Figure S18. Slope (A, left) and aspect (B, right) QRs for the Pozo catchment (see Figure 9 for location).

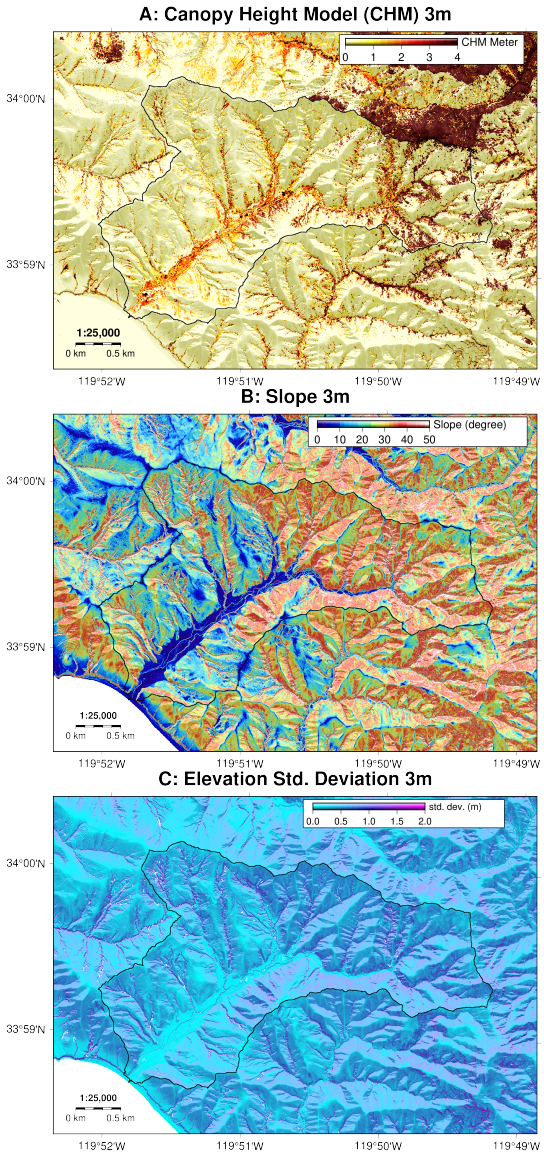

Figure S19. (A) Canopy height, (B) slope, and (C), elevation STD for the Pozo catchment (see Figure 10 for location). Standard deviation is more influenced by terrain slope than vegetation height.

5.4 Identification of Optimal Grid Resolution

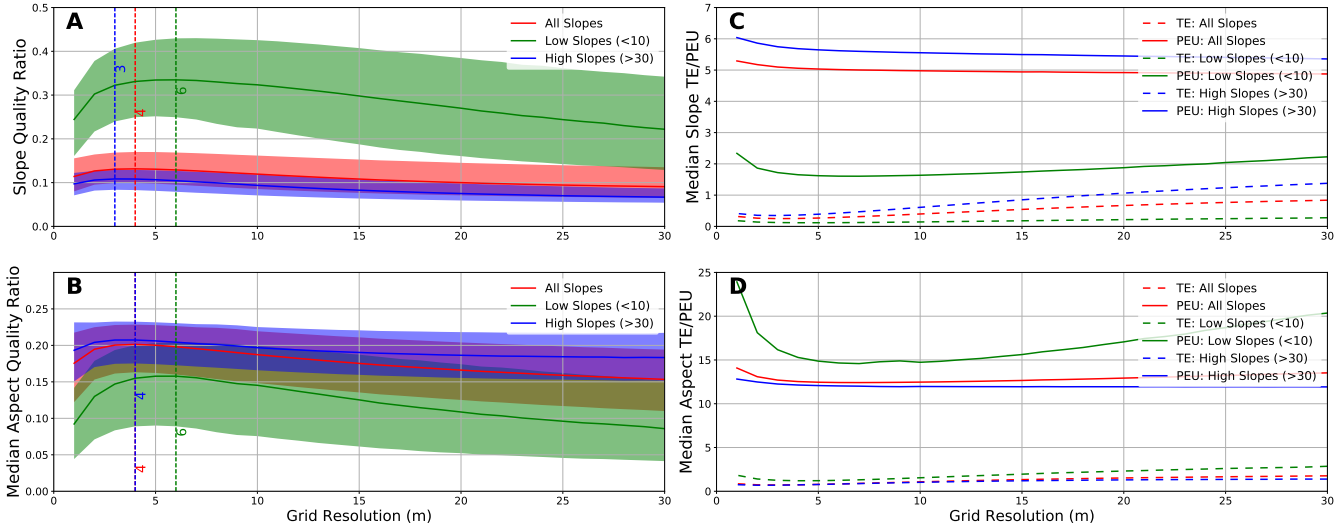

Figure S20. Median Quality Ratios (QRs) for all slopes, low slopes (<10) and high slopes (>30), with inter-quartile range shading. There is a clear slope bias where low slopes have better slope QRs, but worse aspect QRs. The optimal grid resolution for SCI is 4m for both slope and aspect.

Table S1. Whole Island Uncertainty, TE, PEU, and QR statistics for each grid spacing.

Grid Spacing	1m	2m	3m	4m	5m	6m	7m	8m	9m	10m
Median Elevation STD	0.16	0.33	0.49	0.64	0.8	0.96	1.11	1.26	1.41	1.57
Median Slope TE	0.319	0.263	0.249	0.253	0.267	0.288	0.312	0.338	0.366	0.397
Median Slope PEU	5.29	5.17	5.1	5.06	5.03	5.02	5	4.99	4.98	4.98
Median Slope QR	0.114	0.127	0.131	0.131	0.131	0.129	0.127	0.124	0.122	0.119
Median Aspect TE	0.862	0.74	0.72	0.743	0.787	0.841	0.901	0.961	1.02	1.08
Median Aspect PEU	14.1	13.1	12.7	12.5	12.5	12.4	12.4	12.4	12.4	12.5
Median Aspect QR	0.176	0.195	0.2	0.201	0.2	0.198	0.196	0.193	0.19	0.187

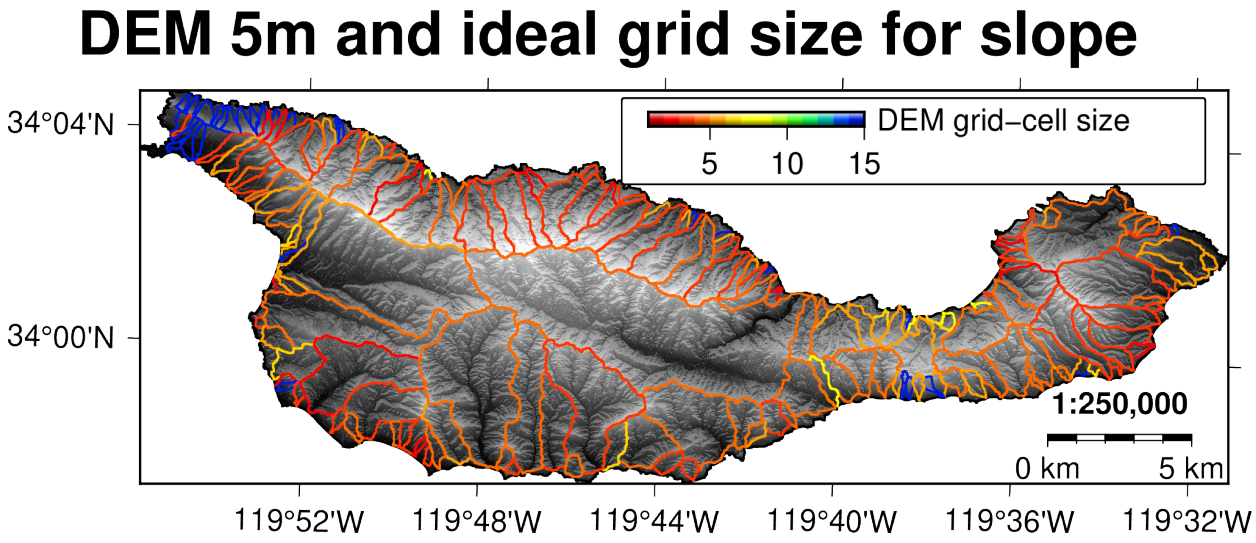

Figure S21. Optimal grid resolution for slope calculations across SCI. Most catchments have optimal resolutions around 2-5m, although some – particularly one region in the north west – have optimal spacings of more than 15m.

5.5 Bias in Real-World Slope and Aspect Distributions

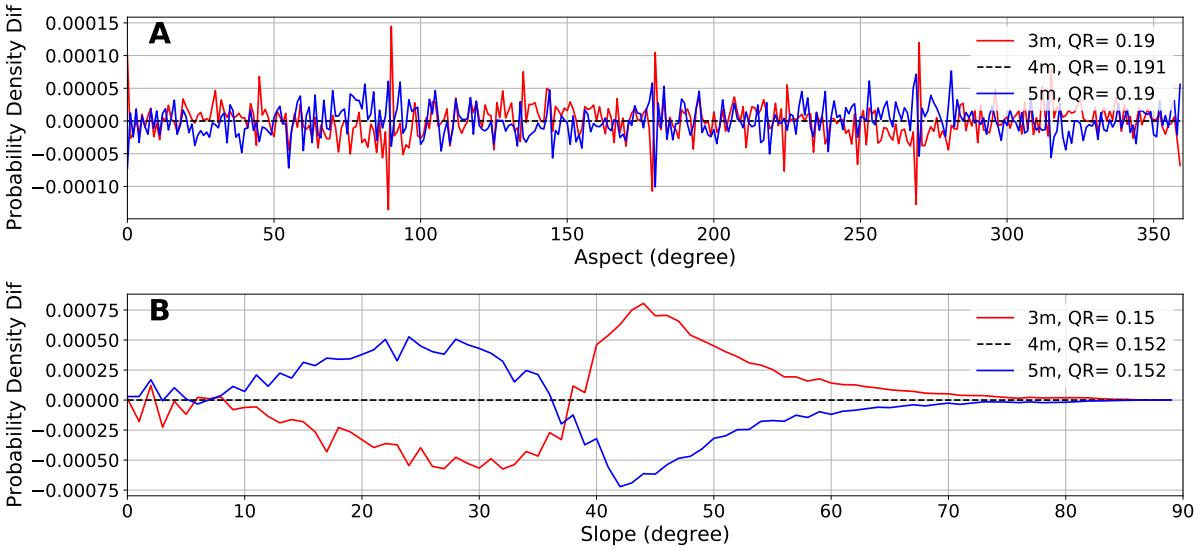

Figure S22. Divergence of high- and low- resolution slope and aspect estimates from the optimal resolution. While the differences in distribution are small, they show a distinct pattern where high slopes are overestimated on high-resolution data, and low slopes are underestimated.

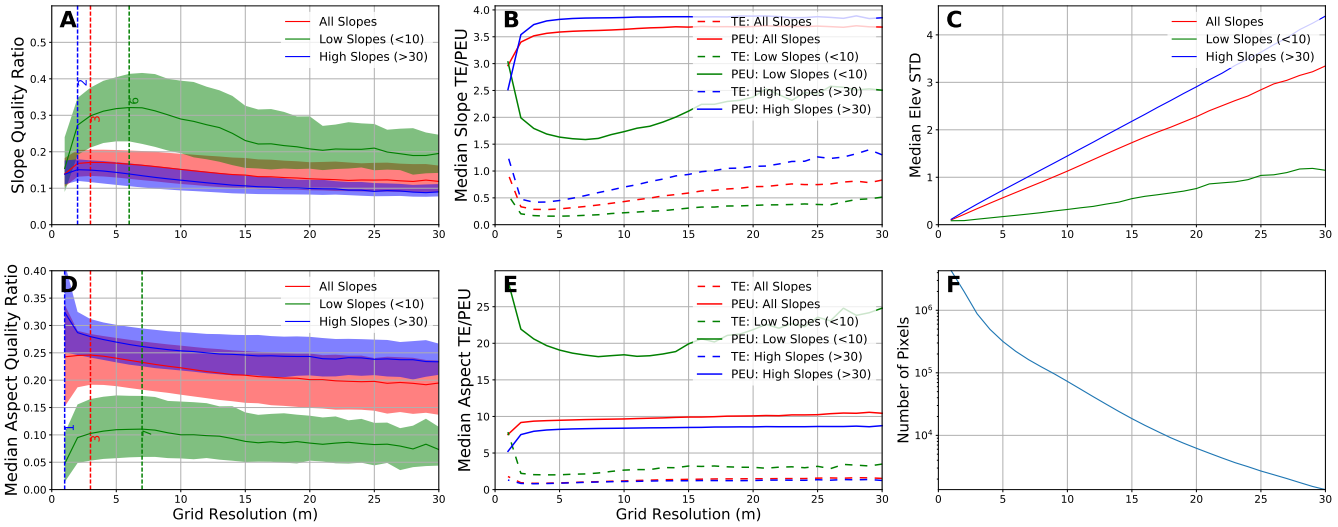

Figure S23. QR for all slopes (red), low slopes (<10, green) and high slopes (>30, blue) for the Pozo catchment (see Figure 10 for location).